Numerical Study of MHD Free Convection in a Packed Bed Square Enclosure Using Local Thermal Non-Equilibrium (LTNE) Model

Ahmed N. Mehdy
Assistant Lecturer
Department of Mechanical Engineering
Engineering college
University of Kufa, Najaf, Iraq

Qahtan AbdulZahra
Assistant Lecturer
Department of Mechanical Engineering
Engineering college
University of Kufa, Najaf, Iraq

Nora M. Sahib
Assistant Lecturer
Department of Computer
Science Teaching College
University of Kufa, Najaf, Iraq

Abstract

In the present study, natural convection of fluid in a square packed bed enclosure is investigated numerically using a uniform magnetic field. The geometry model is heated from left-hand side vertical wall and cooled from opposite wall with adiabatic condition at both the top and bottom walls. Normally to this enclosure an electric coil was set to generate a uniform magnetic field. The Brinkman–Forchheimer extended Darcy model was used to solve the momentum equations, while the energy equations for fluid and solid phase were solved using the local thermal non-equilibrium (LTNE) model. Computations are performed for a range of the Darcy number from 10^{-5} to10^{-1}, the porosity from 0.3 to 0.9, and Hartmann number from 0 to 75. The results showed that both the strength of applied magnetic field and the packed bed characteristics have significant effect on the flow field and heat transfer.

الخلاصة

خلال الدراسة الحالية ، الحمل الحر خلال طبقات محشوة في تجويف مربع تم دراسته عددياً مع تسليط مجال مغناطيسي منتظم. تم تسخين النموذج الهندسي من جهة الجدار العمودي الأيسر وتبريده من الجدار المقابل مع عزل كل من الجدارين العلوي والسفلي . بصورة عمودية على التجويف تم وضع ملف كهربائي لتوليد مجال مغناطيسي منتظم. تم استخدام نموذج برنكمانفورشمايمر المشتق من نموذج دارسي في حل معادلات الزخم ، بينما تم حل معادلات الطاقة لكل من الطورين المائع والصلب باستخدام نموذج عدم الاتزان الحراري الموقعي (LTNE). لقد أنجزت الحسابات لمدى رقم دارسي من 10^{-5} إلى 10^{-1}، المسامية من 0.3 إلى 0.9، وعدد هارتمان من 0 إلى 75 ، لقد أظهرت النتائج بأن كلاً من شدة المجال المغناطيسي المسلط وخصائص الطبقات المحشوة تمتلكان تأثيراً مهماً على حقل الجريان وانتقال الحرارة.

Keywords: Free Convection, MHD, Non-Darcian model, Local thermal non-equilibrium.

Nomenclature

a side length of the enclosure (m)
asf specific surface area of the packed bed (m-1)
B0 uniform magnetic induction (T)
cp specific heat at constant pressure (J kg-1 K-1)
dp sphere particle diameter (m)
Da Darcy number
F geometric function
FM magnetic force
g gravitational acceleration (m s-2)
hsf solid-fluid heat transfer coefficient(Wm-2K-1)
Ha Hartmann number
i, j, k x, y, z- coordinates unit vector
J current density (Amp m-2)
k thermal conductivity (W m-1 K-1)
K permeability (m2)
MHD Magneto hydrodynamic
Nu Nusselt number p pressure (Pa)
P dimensionless pressure
Pr Prandtl number
Ra Rayleigh number
T temperature (K)
u, v velocity components (m s-1)
U, V dimensionless velocity components
x, y x-, y-coordinates (m)
X, Y dimensionless coordinates

Greek symbols

α thermal diffusivity (m2 s-1)
μ viscosity of gas (kg m-1 s-1)
ν kinematic viscosity (m2 s-1)
ρ density (kg m-3)
σ electric conductivity
β thermal expansion coefficient (K-1)
θ dimensionless temperature
ψ dimensionless stream function
ω dimensionless vorticity
Φ general scalar dependent variable
Γ diffusion coeffecient
ε porosity
Λ dimensionless thermal conductivity
ξ dimensionless solid-to-fluid heat transfer coefficient

Subscripts

f fluid
feff effective properties for fluid
i axis indication
m mean value
s solid
seff effective properties for solid
l local value
x x-indication
y y-indication

1- Introduction

Natural convection in MHD flows in packed bed is encountered in a number of problems with technological and scientific interest, which is covering a wide range of basic sciences such as metallurgy, crystal growth and nuclear engineering. Natural convection flows are characterized by a balance between pressure drop and buoyancy forces, in MHD natural convection flows in packed bed, the balance is achieved by inertial, viscous, electromagnetic and buoyancy forces, making the solution is more complicated. The unsteady free convection flow of an electrically conducting fluid between two heated vertical parallel plates with the presence of a magnetic field was investigated by Walker [1] and Singha and Deka [2]. Makinde and Mhone [3] investigated the combined effect of a transverse magnetic field and a radiative heat transfer to unsteady free convective flow through a channel filled with porous medium. MHD free convective flow past a vertical porous plate was analyzed in the presence of a constant suction velocity which is normal to the porous wall by Pillai et. al. [4] and Murthy et. al. [5]. Singh [6] studied the free convection and mass transfer flow of an electrically conducting fluid past a moving vertical porous plate in presence of large suction and under a uniform magnetic field, also in a close field, a study of MHD free convective flow past an infinite vertical oscillating plate through a porous medium was carried out by Chaudhary and Jain [7]. Piazza and Ciofalo [8] investigated numerically the MHD buoyant flow in a cubic enclosure with differential heating at two of the enclosure walls, After that the same investigators studied the same field but with internal heating [9]. Sarris et. al. [10] studied numerically the MHD free convection flows in circular annular cavities and square cavities. Amiri and Vafai [11] presented a numerical transient simulation of incompressible flow through a packed bed by using (LTNE) model. Wang et. al. [12] presented a numerical investigation of natural convection of fluid in an inclined square enclosure filled with porous medium and submitted to a strong magnetic field. However, the magnetic force has received more attention in the field of metallic materials, and less in the field of non-metallic materials. With the increase of magnetic field intensity, the magnetic force has more effects on the nonmetallic materials. The application of strong magnetic field may be found in the field of medical treatment such as magnetic resonance imaging, while the applications of natural convection in porous medium may be found in nuclear reactors, cooling of radioactive waste containers, heat

exchangers, solar power collectors, grain storage, food processing, energy efficient drying process. So, we intend to study the effects of magnetic force on the natural convection in a square packed bed enclosure. The heat and flow characteristics will be studied on the effect of the packed bed parameters and the intensity of magnetic field.

2- Mathematical Model

2.1- Geometrical Shape of Studied Problem

The schematic view of the studied problem is shown in Fig.1. The square enclosure has a side length (a) and it is filled with a saturated packed bed was made from steel. The left vertical wall of the square enclosure is isothermally heated and the opposite wall is isothermally cooled while the other walls are thermally insulated. A uniform magnetic field is applied on the enclosure which be normal to both (x & y) directions as shown in Fig.1.

2.2- Governing Equations

In the model development, the following assumptions are adopted; the working fluid is mercury of Prandtl number Pr=0.025 and assumed to be incompressible and Newtonian fluid, no phase change occurs and the process is in a steady state, the Boussinesq approximation for buoyancy is adopted, the applied magnetic field is uniform throughout the enclosure, low magnetic Reynolds model is assumed where the induced magnetic field is neglected in comparison with the applied magnetic field, the effect of magnetic field on heating is negligible. The Brinkman–Forchheimer extended Darcy model is used to solve the momentum equations while the energy equations for fluid and solid phases are solved with the local thermal non-equilibrium (LTNE) model. Thus, the governing equations for the present study will take the following forms (Amiri & Vafai [11]);

- Continuity equation

$$\frac{\partial u}{\partial x}+\frac{\partial v}{\partial y}=0 \tag{1}$$

- Momentum equations

$$\frac{\rho_f}{\varepsilon^2}\left(u\frac{\partial u}{\partial x}+v\frac{\partial u}{\partial y}\right)=-\frac{\partial p}{\partial x}+\frac{\mu_f}{\varepsilon}\left(\frac{\partial^2 u}{\partial x^2}+\frac{\partial^2 u}{\partial y^2}\right)-\frac{\mu_f}{K}u+\frac{F\,\rho_f\left|\vec{u}\right|u}{\sqrt{K}}+F_{Mx} \tag{2}$$

$$\frac{\rho_f}{\varepsilon^2}\left(u\frac{\partial v}{\partial x}+v\frac{\partial v}{\partial y}\right)=-\frac{\partial p}{\partial y}+\frac{\mu_f}{\varepsilon}\left(\frac{\partial^2 v}{\partial x^2}+\frac{\partial^2 v}{\partial y^2}\right)+\rho_f\, g\,\beta\,(T_f-T_c)-\frac{\mu_f}{K}v+\frac{F\,\rho_f\left|\vec{u}\right|v}{\sqrt{K}}+F_{My} \quad (3)$$

- Fluid phase energy equation

$$\rho_f\, cp_f\left(u\frac{\partial T_f}{\partial x}+v\frac{\partial T_f}{\partial y}\right)=k_{feff}\left(\frac{\partial^2 T_f}{\partial x^2}+\frac{\partial^2 T_f}{\partial y^2}\right)+a_{sf}\,h_{sf}\,(T_s-T_f) \quad (4)$$

- Solid phase energy equation

$$k_{seff}\left(\frac{\partial^2 T_s}{\partial x^2}+\frac{\partial^2 T_s}{\partial y^2}\right)+a_{sf}\,h_{sf}\,(T_f-T_s)=0 \quad (5)$$

the terms (***F*_{*Mx*} & *F*_{*My*}**) in the momentum equations represent the magnetic body forces (Lorentz forces) in (***x* & *y***) directions respectively and they are defined as follow (Tillack and Morley [13]);

$$F_{Mx}=\overrightarrow{J_y}\times\overrightarrow{B_0} \quad \text{i i i } (6.a)$$

$$F_{My}=\overrightarrow{J_x}\times\overrightarrow{B_0} \quad \text{i i i } (6.b)$$

where $\overrightarrow{B_0}$ is the applied magnetic field vector, while $\left(\overrightarrow{J_x}\ \&\ \overrightarrow{J_y}\right)$ represent the current densities due to the magnetic field and they are defined as follow (Tillack and Morley [13]);

$$\overrightarrow{J_y}=\sigma\left(\vec{u}\times\overrightarrow{B_0}\right)=\sigma\left[(u)i\times(B_0)k\right]=(-\sigma\,u\,B_0)\,j \quad \text{i i i } (7.a)$$

$$\overrightarrow{J_x}=\sigma\left(\vec{v}\times\overrightarrow{B_0}\right)=\sigma\left[(v)\,j\times(B_0)k\right]=(\sigma\,v\,B_0)\,i \quad \text{i i i } (7.b)$$

by substituting equations [(7.a) & (7.b)] in equations [(6.a) & (6.b)] respectively we get the final forms of the magnetic body forces as follow;

$$F_{Mx}=(-\sigma\,u\,B_0)\,j\times(B_0)\,k=(-\sigma\,u\,B_0^2)\,i \quad \text{i i i } (8.a)$$

$$F_{My}=(\sigma\,v\,B_0)\,i\times(B_0)\,k=(-\sigma\,v\,B_0^2)\,j \quad \text{i i i } (8.b)$$

The geometric function ***F***, specific surface area of the packed bed $\boldsymbol{a_{sf}}$ and the fluid-to-solid heat transfer coefficient in a packed bed $\boldsymbol{h_{sf}}$ are determined as suggested by (Amiri & Vafai [11]);

$$F = \frac{1.75}{\sqrt{150\ \varepsilon^3}} \qquad \text{i i i } (9.a)$$

$$a_{sf} = \frac{6\,(1-\varepsilon)}{d_p} \qquad \text{i i i } (9.b)$$

$$h_{sf} = k_f \left[2 + 1.1\ \mathrm{Pr}^{1/3} \left(\frac{\rho_f \left| \vec{u} \right| d_p}{\mu_f} \right)^{0.6} \right] \qquad \text{i i i } (9.c)$$

where the sphere particle diameter ***dp*** can be computed as follow (Amiri & Vafai [11]);

$$d_p = (1-\varepsilon)\sqrt{\frac{150\,K}{\varepsilon^3}} \qquad \text{i i i } (9.d)$$

while the effective thermal conductivity $\boldsymbol{k_{feff}}$ and $\boldsymbol{k_{seff}}$ in fluid and solid phase energy equations and the mean thermal diffusivity $\boldsymbol{\alpha_m}$ can be computed as follow (Wang et. al. [12]);

$$k_{feff} = \varepsilon\ k_f \qquad \text{i i i } (10.a)$$

$$k_{seff} = (1-\varepsilon)\,k_s \qquad \text{i i i } (10.b)$$

$$\alpha_m = \frac{k_{feff} + k_{seff}}{\rho_f\, cp_f} \qquad \text{i i i } (10.c)$$

Now we introduce the following non-dimensional quantities and parameters (Wang et. al. [12]);

$$\left.\begin{aligned} X &= \frac{x}{a}, \quad Y = \frac{y}{a} \\ U &= \frac{a\,u}{\alpha_m}, \quad V = \frac{a\,v}{\alpha_m}, \quad P = \frac{p\,a^2}{\rho_f\,\alpha_m{}^2} \\ \theta_f &= \frac{(T_f - T_c)}{(T_h - T_c)}, \quad \theta_s = \frac{(T_s - T_c)}{(T_h - T_c)} \end{aligned}\right\} \qquad \text{i i i } (11.a)$$

$$\left.\begin{aligned} \mathrm{Pr} &= \frac{\mu_f\, cp_f}{k_{feff} + k_{seff}} = \frac{\nu_f}{\alpha_m}, \quad Ra = \frac{g\,a^3\,\beta\,(T_h - T_c)}{\nu_f\,\alpha_m} \\ Da &= \frac{K}{a^2}, \quad Ha = a\,B_0\sqrt{\frac{\sigma_f}{\mu_f}} \\ \Lambda &= \frac{k_{feff}}{k_{seff}}, \quad \xi = \frac{a_{sf}\,h_{sf}\,a^2}{k_{feff}} \end{aligned}\right\} \qquad \text{i i i } (11.b)$$

By substituting equations [(11.a)&(11.b)] in equations [(1),(2),(3),(4)&(5)], we get the dimensionless forms of governing equations as follow;

$$\frac{\partial U}{\partial X}+\frac{\partial V}{\partial Y}=0 \qquad \text{i i i (12)}$$

$$\frac{1}{\varepsilon^2}\left(U\frac{\partial U}{\partial X}+V\frac{\partial U}{\partial Y}\right)=-\frac{\partial P}{\partial X}+\frac{\Pr}{\varepsilon}\left(\frac{\partial^2 U}{\partial X^2}+\frac{\partial^2 U}{\partial Y^2}\right)-\frac{\Pr}{Da}U-\frac{F\left|\vec{U}\right|U}{\sqrt{Da}}-\Pr Ha^2 U \qquad \text{i (13)}$$

$$\frac{1}{\varepsilon^2}\left(U\frac{\partial V}{\partial X}+V\frac{\partial V}{\partial Y}\right)=-\frac{\partial P}{\partial Y}+\frac{\Pr}{\varepsilon}\left(\frac{\partial^2 V}{\partial X^2}+\frac{\partial^2 V}{\partial Y^2}\right)+\Pr Ra\,\theta_f-\frac{\Pr}{Da}V-\frac{F\left|\vec{U}\right|V}{\sqrt{Da}}-\Pr Ha^2 V \qquad \text{i (14)}$$

$$\left(1+\Lambda^{-1}\right)\left(U\frac{\partial \theta_f}{\partial X}+V\frac{\partial \theta_f}{\partial Y}\right)=\left(\frac{\partial^2 \theta_f}{\partial X^2}+\frac{\partial^2 \theta_f}{\partial Y^2}\right)+\xi\,(\theta_s-\theta_f) \qquad \text{i i i (15)}$$

$$0=\left(\frac{\partial^2 \theta_s}{\partial X^2}+\frac{\partial^2 \theta_s}{\partial Y^2}\right)+\Lambda\xi\,(\theta_f-\theta_s) \qquad \text{i i i (16)}$$

Using the (stream function-vorticity) formulation, the dependent variables will be reduced to only four variables, by differentiating equation (13) with respect to (Y) and differentiating equation (14) with respect to (X), after that, the first of the two resulted equations is subtracted from the second to eliminate the pressure terms from the momentum equations, thus, equations [(12),(13)&(14)] will be transformed to the following equations;

$$\frac{\partial^2 \psi}{\partial X^2}+\frac{\partial^2 \psi}{\partial Y^2}=-\omega \qquad \text{i i i (17)}$$

$$U\frac{\partial \omega}{\partial X}+V\frac{\partial \omega}{\partial Y}=\varepsilon\,\Pr\left(\frac{\partial^2 \omega}{\partial X^2}+\frac{\partial^2 \omega}{\partial Y^2}\right)+\varepsilon^2\left[\Pr Ra\frac{\partial \theta}{\partial X}-\left(\Pr Ha^2+\frac{\Pr}{Da}+\frac{F\left|\vec{U}\right|}{\sqrt{Da}}\right)\omega-\frac{F}{\sqrt{Da}}\left(V\frac{\partial\left|\vec{U}\right|}{\partial X}-U\frac{\partial\left|\vec{U}\right|}{\partial Y}\right)\right] \qquad \text{i i (18)}$$

where (ψ&ω) are the (stream function & vorticity) respectively, and they are defined as follow;

$$U=\frac{\partial \psi}{\partial Y}\ \&\ V=-\frac{\partial \psi}{\partial X} \qquad \text{i i i (19.}a\text{)}$$

$$\omega=\frac{\partial V}{\partial X}-\frac{\partial U}{\partial Y} \qquad \text{i i i (19.}b\text{)}$$

After getting the final values of all dependent variables in the flow field, calculations will be made for local and mean Nusselt number, where the local Nusselt number at the hot wall can be found as follow (Wang et. al [12]);

$$Nu_l=\varepsilon\left(\left.\frac{\partial \theta_f}{\partial X}\right|_{X=0}+\Lambda^{-1}\left.\frac{\partial \theta_s}{\partial X}\right|_{X=0}\right) \qquad \text{i i i (20)}$$

2.3- Boundary Conditions

The hydrodynamic boundary conditions for the present problem at all enclosure walls will obey to the non-slip condition, while the thermal boundary conditions are (the left side wall was kept hot, the right side wall was kept cold and finally each one of the top and bottom walls were kept isothermally insulated), thus the boundary conditions will be as follow;

$$\left.\begin{array}{ll} U=0, V=0, \theta_f=\theta_s=1 & at\ X=0; \\ U=0, V=0, \theta_f=\theta_s=0 & at\ X=1; \\ U=0, V=0, \dfrac{\partial\theta_f}{\partial Y}=\dfrac{\partial\theta_s}{\partial Y}=0 & at\ Y=0\ \&\ 1 \end{array}\right\} \qquad \text{i i i (21)}$$

3- Numerical Solution

The governing equations for (ψ, ω, θ_f & θ_s) can be written in a common form for the (convection-diffusion) problem as follow (Versteeg and Malalasekera [14]);

$$\frac{\partial}{\partial X_i}(\rho\, u_i \Phi)=\frac{\partial}{\partial X_i}\left(\Gamma\frac{\partial\Phi}{\partial X_i}\right)+S \qquad \text{i i i (22)}$$

where the general scalar $\boldsymbol{\Phi}$ stands for any one of the dependent variables under consideration, the diffusion coeffecient $\boldsymbol{\Gamma}$ and the source term $\boldsymbol{S}$ in cartesian form are listed below for each governing equation;

- Stream function equation

$$\Phi=\psi,\ \Gamma=1,\ S=\omega \qquad \text{h h h (23.}a\text{)}$$

- Vorticity equation

$$\Phi=\omega,\ \Gamma=\varepsilon\ \mathrm{Pr},\ S=\varepsilon^2\left[\mathrm{Pr}\,Ra\frac{\partial\theta}{\partial X}-\left(\mathrm{Pr}\,Ha^2+\frac{\mathrm{Pr}}{Da}+\frac{F\left|\vec{U}\right|}{\sqrt{Da}}\right)\omega - \frac{F}{\sqrt{Da}}\left(V\frac{\partial\left|\vec{U}\right|}{\partial X}-U\frac{\partial\left|\vec{U}\right|}{\partial Y}\right)\right] \qquad \text{h h h (23.}b\text{)}$$

- Fluid phase energy equation

$$\Phi=\theta_f,\ \Gamma=\frac{1}{1+\Lambda^{-1}},\ S=\frac{\xi\,(\theta_s-\theta_f)}{1+\Lambda^{-1}} \qquad \text{h h h (23.}c\text{)}$$

- Solid phase energy equation

$$\Phi=\theta_s,\ \Gamma=1,\ S=\Lambda\,\xi\,(\theta_f-\theta_s) \qquad \text{h h h (23.}d\text{)}$$

The numerical solution of the governing equations will be made according to the finite volume method to transform the governing equations from partial differential

form to discrete algebraic form, this method is based on principle of dividing the flow field to a number of volume elements, each one of them is called (control volume), after that a discretization process (Versteeg and Malalasekera [14]) was carried out by integrating the general conservation equation (22) over a control volume element, where this equation will be as follow;

$$a_P \Phi_P = a_E \Phi_E + a_W \Phi_W + a_N \Phi_N + a_S \Phi_S + S_u \qquad \text{i i i (24)}$$

where;

$$a_P = a_E + a_W + a_N + a_S - S_P \qquad \text{i i i (25)}$$

the source coefficients (S_u & S_p) represent the source terms of the discrete equation and their values for each governing equation are listed as follow;

- For the stream function equation

$$\left.\begin{aligned} S_u &= \omega \\ S_p &= 0 \end{aligned}\right\} \qquad \text{i i i (26.}a\text{)}$$

- For the vorticity equation

$$\left.\begin{aligned} S_u &= \varepsilon^2 \left[\Pr\, Ra \frac{\partial \theta}{\partial X} - \frac{F}{\sqrt{Da}} \left(V \frac{\partial |\vec{U}|}{\partial X} - U \frac{\partial |\vec{U}|}{\partial Y} \right) \right] \\ S_p &= -\varepsilon^2 \left(\Pr\, Ha^2 + \frac{\Pr}{Da} + \frac{F |\vec{U}|}{\sqrt{Da}} \right) \end{aligned}\right\} \qquad \text{i i i (26.}b\text{)}$$

- Fluid phase energy equation

$$\left.\begin{aligned} S_u &= \frac{\xi\, \theta_s}{1 + \Lambda^{-1}} \\ S_p &= -\frac{\xi}{1 + \Lambda^{-1}} \end{aligned}\right\} \qquad \text{i i i (26.}c\text{)}$$

- Solid phase energy equation

$$\left.\begin{aligned} S_u &= \Lambda\, \xi\, \theta_f \\ S_p &= -\Lambda\, \xi \end{aligned}\right\} \qquad \text{i i i (26.}d\text{)}$$

A computational program was written in Fortran-90 language to compute the values of the required variables, The discretized algebraic equations are solved by the tri-diagonal matrix algorithm (TDMA). Relaxation factors of about (0.5–0.7) are used for all dependent variables, Convergence was measured in terms of the maximum change in each variable during an iteration where the maximum change allowed for convergence check was (10^{-6}).

4- Results and Discussion

All results were carried out for mercury at ($Ra = 10^4$), where the results show that the flow and temperature field are very affected with the characteristics of both the applied magnetic field and the packed bed. Figs.(2, 3 & 4) show the effect of Darcy number on the stream function, fluid temperature and solid temperature contours respectively at low Hartmann number (Ha=25). Fig.(2.a) explains the stream function contour at low Darcy number ($Da=10^{-5}$), and as a result of the buoyancy effect, the fluid at the left-hand side hot wall will be lighter than it in other locations while the fluid at the right-hand side cold wall will be heavier than it in other locations, so, the fluid particles move upward along the hot wall while they move downward along the cold wall, and thus, the flow will take the direction of counterclockwise, After that and with increasing Darcy number as in Figs.[(2.b) & (2.c)] the flow levels will increase because of the increasing in the volume of passable paths of fluid through the packed bed, so, the overall packed bed resistance to the flow will decrease. Fig.(3.a) explains the fluid phase temperature contour for low Darcy number ($Da=10^{-5}$), and as it is clear that the thermal levels will decrease longitudinally from the left-hand side hot wall to the right-hand side cold wall, After that and with increasing Darcy number as in Figs.[(3.b) & (3.c)] the temperature levels will increase gradually, where the hot fluid rises up along the left-hand side hot wall and descends along the right-hand side cold wall because of the buoyancy effect. Fig.(4) explains the solid phase temperature contours at different values of Darcy number, where it is noted that the distribution of solid phase temperature will comport in a similar behavior to distribution of fluid phase temperature, but the temperatures levels will be less than them in fluid phase because of the absence of convection terms in the solid phase energy equation. Figs.(5, 6 & 7) show the effect of Darcy number on the stream function, fluid temperature and solid temperature contours respectively at high Hartmann number (Ha=75), where it is noted that the distributions of stream function and temperatures for both the fluid and solid phases at high Hartmann number will comport in a similar behavior to their distributions at low Hartmann number, but their levels will be less than them at low Hartmann number because of the strong effects of the magnetic force on the flow which will be opposite to the flow direction. Figs.(8, 9 & 10) show the effect of porosity on the stream function, fluid temperature and solid temperature contours respectively at low Hartmann number (Ha=25). Fig.(8.a) explains the stream function contour at low porosity ($\varepsilon=0.4$), where the flow will take the direction of counterclockwise for the same mentionable reason previously, After that and with

increasing the porosity as in Figs.[(8.b) & (8.c)] the flow levels will increase because of the decreasing in the occupied volume by the bed through enclosure, so, the overall packed bed resistance to the flow will decrease. Fig.(9.a) explains the fluid phase temperature contour for low porosity (ε=0.4), and as it is clear that the hot fluid rises up along the left-hand side hot wall and descends along the right-hand side cold wall because of the buoyancy effect, After that and with increasing the porosity as in Figs.[(9.b) & (9.c)] the temperature distribution will comport in a similar behavior to its distribution at low porosity, but the temperatures levels will be more than them in low porosity because of the increasing in the source of fluid phase energy equation Eq.(23.c) as a result of increase in both the dimensionless thermal conductivity Λ and the dimensionless solid-to-fluid heat transfer ξ with porosity increase. Fig.(10) explains the solid phase temperature contours at different values of porosity, where the distribution of solid phase temperature will be analogous to the distribution of fluid phase temperature and for the same mentionable reason previously, but it was noted that the thermal levels at low porosity (ε=0.4) will decrease longitudinally from the left-hand side hot wall to the right-hand side cold wall. Figs.(11, 12 & 13) show the porosity effect on the stream function, fluid temperature and solid temperature contours respectively at high Hartmann number (Ha=75), where it is noted that the distributions of stream function and temperatures for both the fluid and solid phases at high Hartmann number will comport in a similar behavior to their distributions at low Hartmann number, but their levels will be less than them at low Hartmann number because of the strong effects of the magnetic force on the flow which will be opposite to the flow direction. Fig.(14.a) explains the effect of Darcy number on the local Nusselt number at a low Hartmann number (Ha=25) and as it is clear that the value of local Nusselt number be maximum at the bottom of the left-hand vertical wall and it decreases gradually with rising to the wall top because the temperature gradient will be very strong at the bottom and it decreases gradually to the top, Also it is clear the increasing in the local Nusselt number levels with Darcy number increase, After that and with Hartmann number increase (Ha=75) as in Fig.(14.b) the local Nusselt number holds the same previous behavior but its levels will be less because of the strong effect of the magnetic forces. Fig.(15.a) explains the effect of porosity on the local Nusselt number at a low Hartmann number (Ha=25) and as in Fig.(14.a) the value of local Nusselt number be maximum at the bottom of the right-hand vertical wall and it decreases gradually with rising to the wall top and for the same mentionable reason previously and with increasing Hartmann number (Ha=75) as in Fig.(15.b) the local Nusselt number nearly holds the same previous behavior but its

levels will be less because of the strong effect of the magnetic forces. Fig.(16) describes the variation of mean Nusselt number with both Hartmann number and Darcy number, where it was noted that the mean Nusselt number generally increases with Darcy number increase because of the decreasing in whole bed resistance to the flow inside it while it decreases with Hartmann number increase because of the increasing in generated magnetic forces inside the flow which shall be opposite to the flow direction. Fig.(17) describes the variation of mean Nusselt number with both Hartmann number and the porosity, at no applied magnetic field (Ha=0) or low Hartman number (Ha=25) it was noted that at porosity range of (ε=0.4-0.7), the value of mean Nusselt number increases gradually with the increase of porosity in that range, but when the porosity increases above that range, the value of mean Nusselt number will decrease, and for explaining this phenomenon clearly we must return to Eq.(20), where it is noted that the whole value of local Nusselt number is multiplicand by the porosity while the second term in this equation (solid phase term) was multiplicand by the inverse of dimensionless thermal conductivity Λ^{-1} which decreases with the increase of porosity $\left[\Lambda^{-1} = (1-\varepsilon)\, k_s / \varepsilon\, k_f\right]$, so, when the porosity values equal to or less than (0.7), the value of local Nusselt number will increase, while it decreases after that value of porosity because the value of dimensionless thermal conductivity will be very small and it causes decreasing in Nusselt number more than the increasing in it because of porosity, After that with increasing in Hartmann number, we note that the levels of mean Nusselt number will decrease, also we note that at high Hartmann number (Ha=75), the value of Nusselt number decreases with increase of porosity because the magnetic forces will increase due to the increase of fluid volume with increase of porosity. To exhibit the reliability of the presented results, the variation of mean Nusselt number with Darcy number at (Ha=0 & ε=0.9) were compared with results of Wang et. al. [12] at the same conditions as shown in Fig.(18), where it is clear the similarity in Nusselt number behavior with the mentionable study but there is a small difference between these values because of the difference in both working fluid and bed material of the compared studies.

5- Conclusions

This paper has presented a numerical investigation of MHD natural convective flow in a packed bed square enclosure by using local thermal non-equilibrium (LTNE) model, and from the resulted data we conclude the following points;

5.1- Generally, both the levels of flow and heat transfer decrease with the increase of Hartmann number as a result of increasing in magnetic forces.

5.2- The value of mean Nusselt number increases with increase of Darcy Number at each Hartmann number values.

5.3- At low Hartmann numbers, the value of mean Nusselt number increases with increase of porosity until the porosity reaches a certain value of about ($\varepsilon \approx 0.6$-0.7) where the value of mean Nusselt number will decrease after that value of porosity, while at high Hartmann numbers, the value of mean Nusselt number will decreases after a porosity value less than the mentionable value previously.

References

[1] Walker, J. S., Magnetohydrodynamic flows in rectangular ducts with thin conducting walls. Journal de Méchanique 20(1), 79-112, 1981.

[2] Krishna Gopal Singha* and P. N. Deka†, Skin-friction for unsteady free convection MHD flow between two heated vertical parallel plates, Theoret. Appl. Mech., Vol.33, No.4, pp. 259-280, Belgrade, 2006.

[3] O. D. Makinde[1] and P. Y. Mhone, Heat transfer to MHD oscillatory flow in a channel filled with porous medium, Journ. Phys., Vol. 50, Nos. 9-10, P. 931-938, Bucharest, 2005.

[4] K. Jagadeeswara Pillai, S. Vijaya Kumar Varma and M. Syam Babu, MHD free convective flow past a hot vertical porous plate, Def. Sci. J., Vol. 37, No. 3, pp. 327-332, July 1987.

[5] M. V. Ramana Murthy[1], G. Noushima Humera[2], Rafiuddin[2] and M. Chenna Krishan Reddy[1], MHD unsteady free convective Walter's memory flow with constant suction and heat sink, ARPN Journal of Engineering and Applied Sciences, Vol. 2, No. 5, October 2007.

[6] Atul Kumar Singh*, MHD free convection and mass transfer flow with heat source and thermal diffusion, Journal of Energy, Heat and Mass Transfer, vol. 23, pp. 227-249, 2001.

[7] R. C. Chaudhary and Arpita Jain, Combined heat and mass transfer effects on MHD free convection flow past an oscillating plate embedded in porous medium, Journ. Phys., Vol. 52, Nos. 5–7, P. 505–524, Bucharest, 2007.

[8] Di Piazza I. and Ciofalo M., "MHD free convection in a liquid-metal filled cubic enclosure. - I. Differential heating". Submitted to International Journal of Heat and Mass Transfer, 2000.

[9] Ivan Di Piazza† and Michele Ciofalo‡, "MHD free convection in a liquid-metal filled cubic enclosure. - II. Internal heating", Int. J. Heat Mass Transfer, Vol.45, No.7, pp.1493-1511, 2002.

[10] I. E. Sarris, S. C. Kakarantzas, A. P. Grecos and N. S. Vlachos, Modeling MHD free convection flows of liquid metals in cavities, 6th Fusion School 2007 –Volos 26-31, March 2007.

[11] A. Amiri and K. Vafai, Transient analysis of incompressible flow through a packed bed, International Journal of Heat and Mass Transfer, 41, 4259-4279, 1998.

[12] Q. W. Wang*, M. Zeng, Z. P. Huang, G. Wang, H. Ozoe, Numerical investigation of natural convection in an inclined enclosure filled with porous medium under magnetic field, International Journal of Heat and Mass Transfer 50, 3684-3689, 2007.

[13] M. S. Tillack and N. B. Morley, Magnetohydrodynamics, 14th edition, McGraw Hill, 1998.

[14] Versteeg H. K. and Malalasekera W., An introduction to computational fluid dynamics the finite volumes method, Longman Group Ltd, 1995.

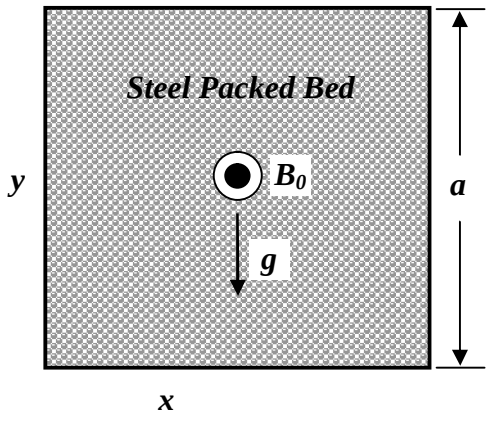

Fig.(1) schematic diagram of the physical system

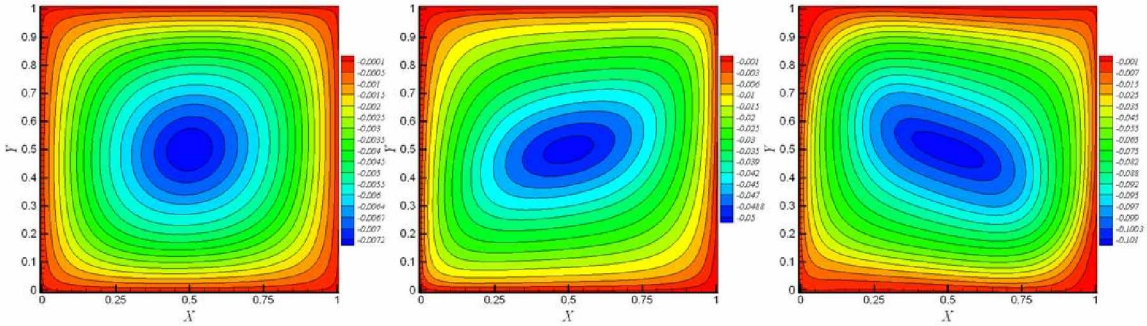

a) Da= 1.E-5 **b) Da= 1.E-3** **c) Da= 1.E-1**

Fig. (2) Streamlines distribution at; Ha=25 & ε=0.8

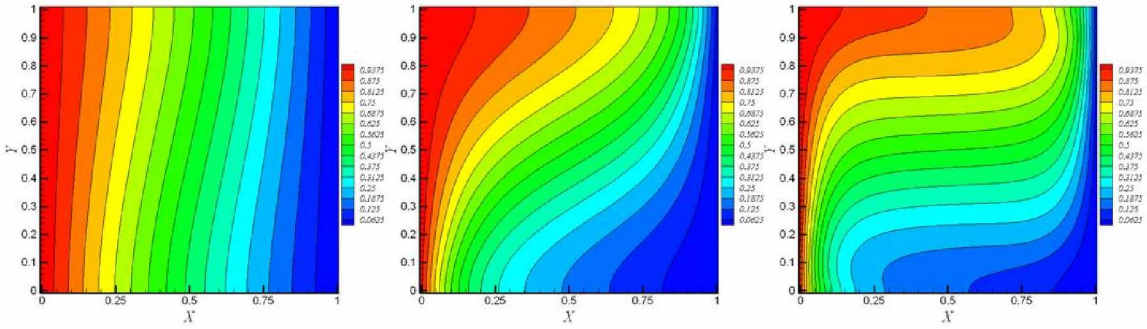

a) Da= 1.E-5 **b) Da= 1.E-3** **c) Da= 1.E-1**

Fig. (3) Temperature distribution of the fluid phase at; Ha=25 & ε=0.8

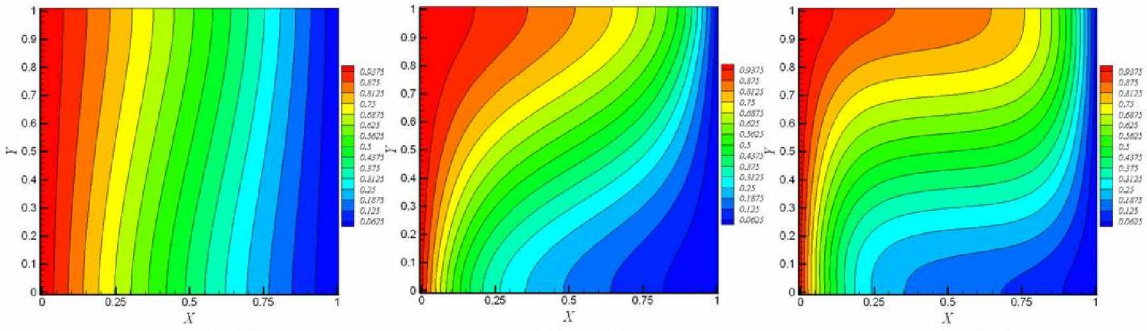

a) Da= 1.E-5 **b) Da= 1.E-3** **c) Da= 1.E-1**

Fig. (4) Temperature distribution of the solid phase at; Ha=25 & ε=0.8

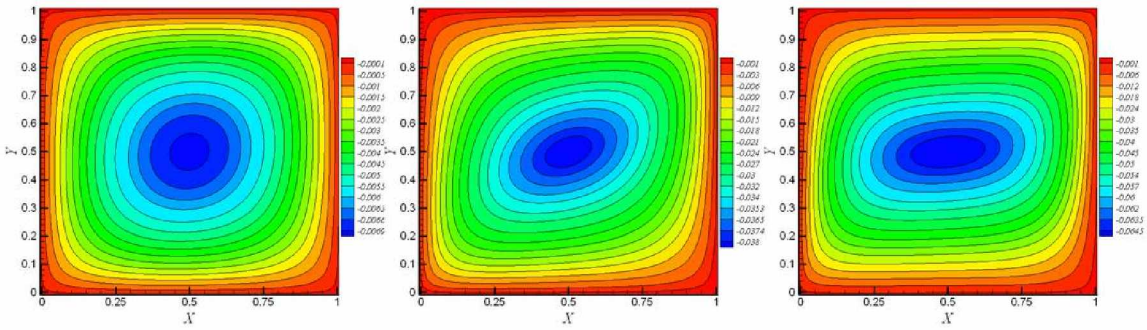

a) Da= 1.E-5 **b) Da= 1.E-3** **c) Da= 1.E-1**

Fig. (5) Streamlines distribution at; Ha=75 & ε= 0.8

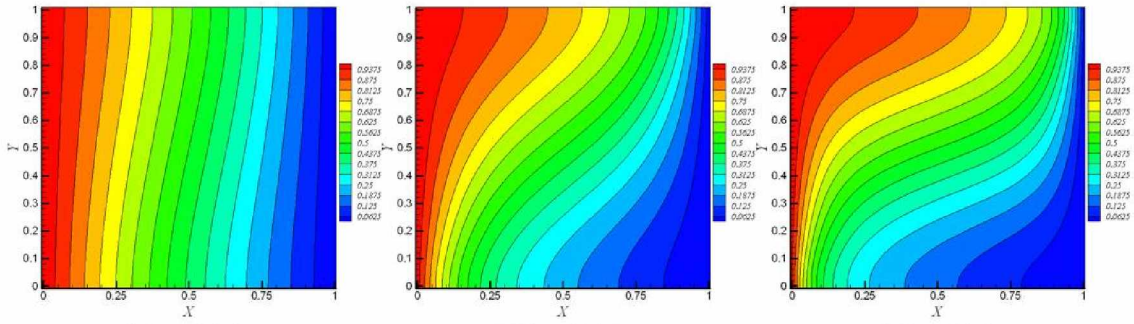

a) Da= 1.E-5 **b) Da= 1.E-3** **c) Da= 1.E-1**

Fig. (6) Temperature distribution of the fluid phase at; Ha=75 & ε= 0.8

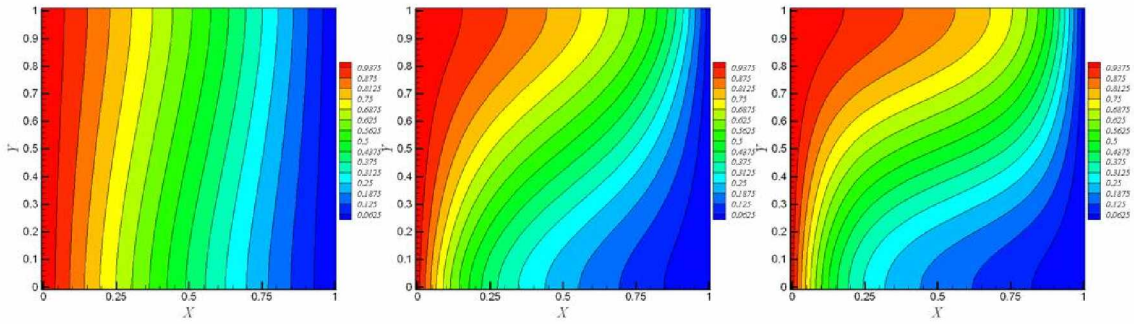

a) Da= 1.E-5 **b) Da= 1.E-3** **c) Da= 1.E-1**

Fig. (7) Temperature distribution of the solid phase at; Ha=75 & ε= 0.8

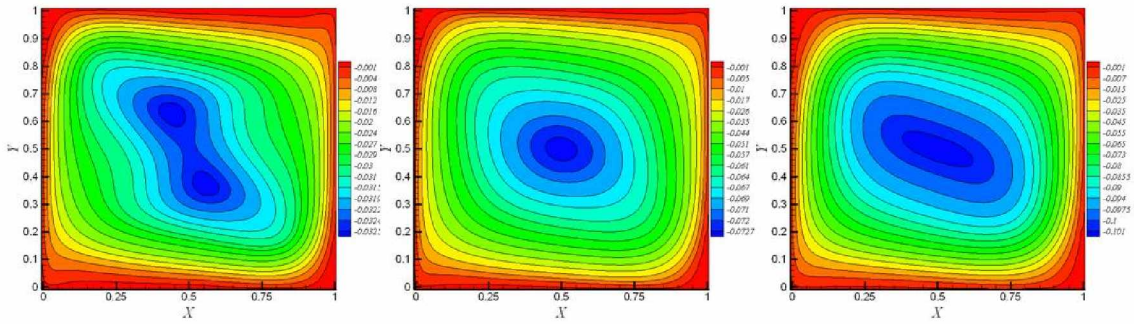

a) ε= 0.4 **b) ε= 0.6** **c) ε= 0.8**

Fig. (8) Streamlines distribution at; Ha=25 & Da=1.E-3

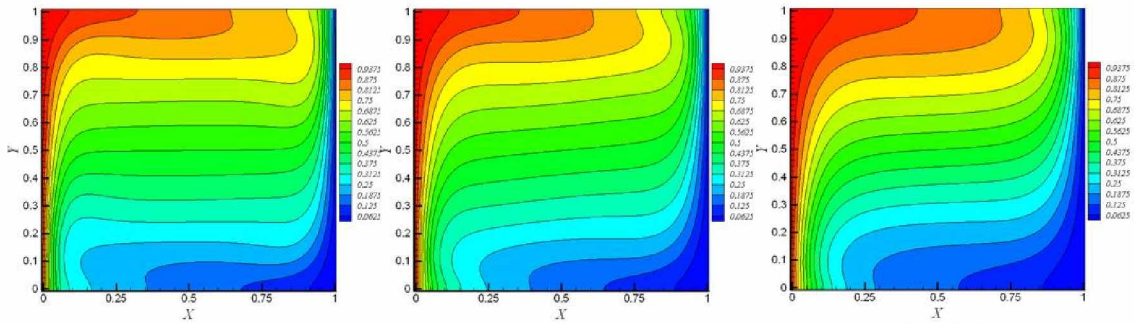

a) ε= 0.4 **b) ε= 0.6** **c) ε= 0.8**

Fig. (9) Temperature distribution of the fluid phase at; Ha=25 & Da=1.E-3

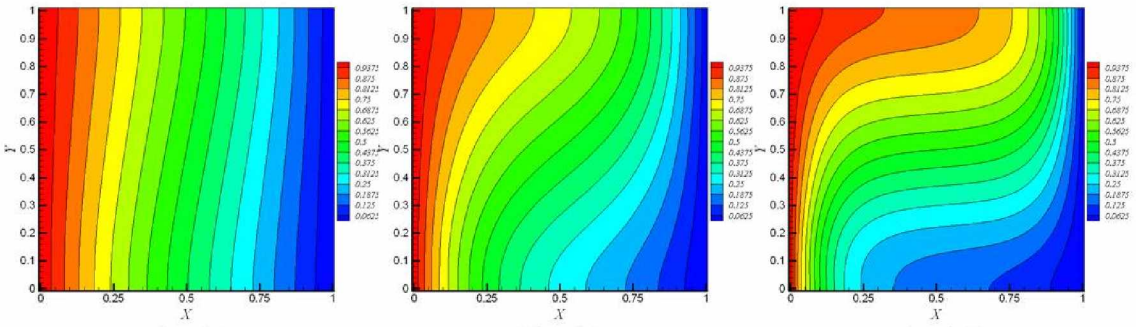

a) ε= 0.4 **b) ε= 0.6** **c) ε= 0.8**

Fig. (10) Temperature distribution of the solid phase at; Ha=25 & Da=1.E-3

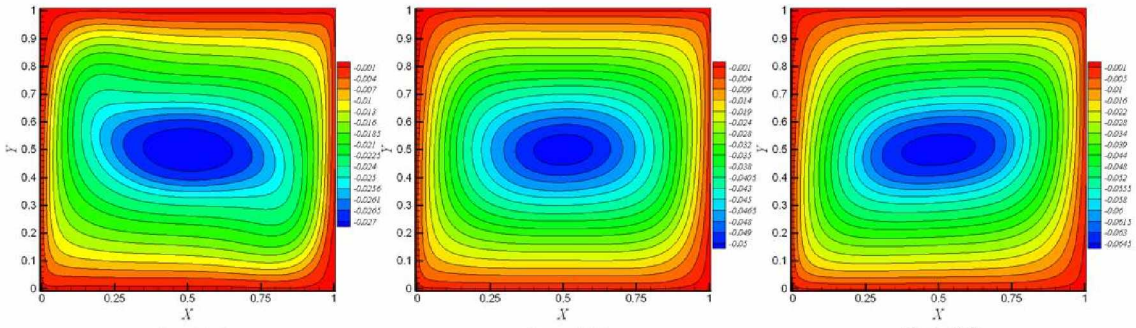

a) ε= 0.4 **b) ε= 0.6** **c) ε= 0.8**

Fig. (11) Streamlines distribution at; Ha=75 & Da=1.E-3

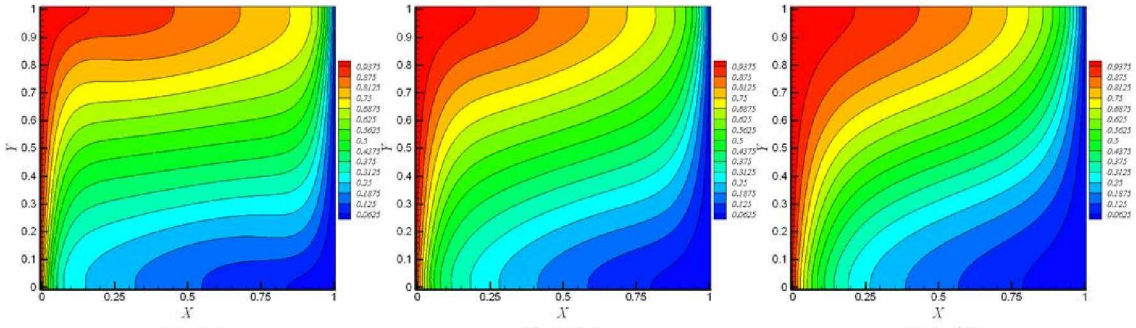

a) ε= 0.4 **b) ε= 0.6** **c) ε= 0.8**

Fig. (12) Temperature distribution of the fluid phase at; Ha=75 & Da=1.E-3

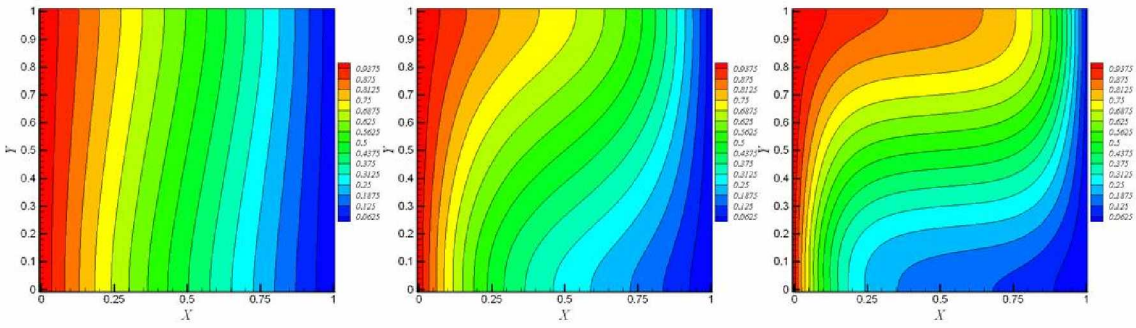

a) ε= 0.4 **b) ε= 0.6** **c) ε= 0.8**

Fig. (13) Temperature distribution of the solid phase at; Ha=75 & Da=1.E-3

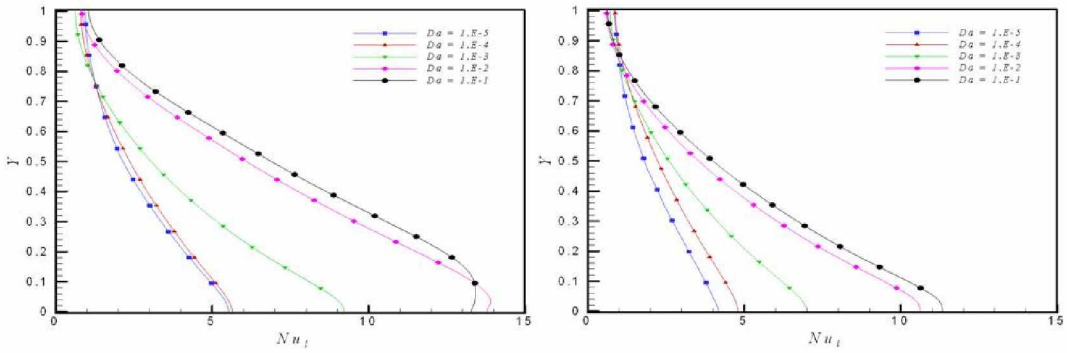

a) Ha= 25 **b) Ha= 75**

Fig. (14) Variation of local Nusselt number with Darcy number at ε=0.8

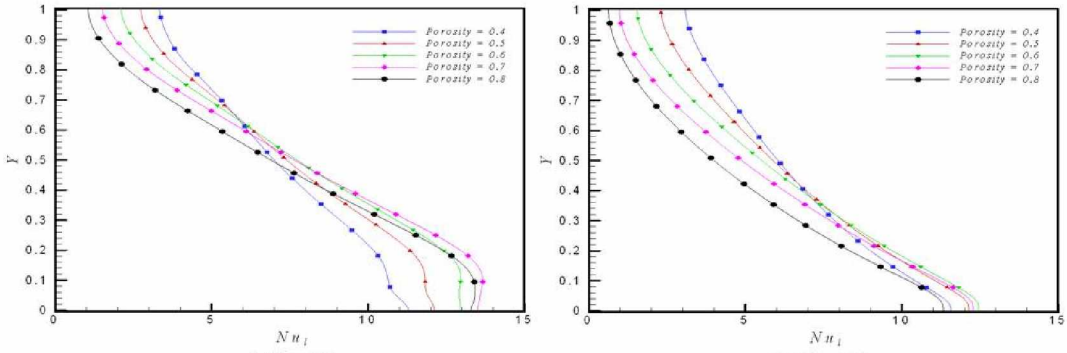

a) Ha= 25 **b) Ha= 75**

Fig. (15) Variation of local Nusselt number with porosity at Da=1.E-3

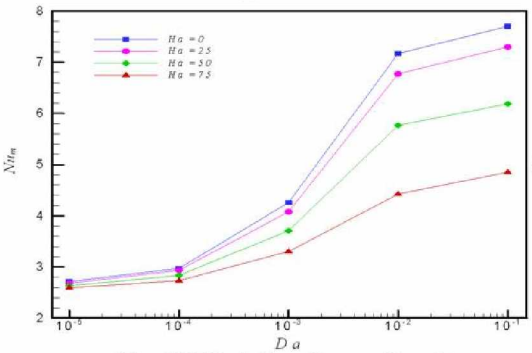

Fig. (16) Variation of mean Nusselt number with Darcy number at ε=0.8

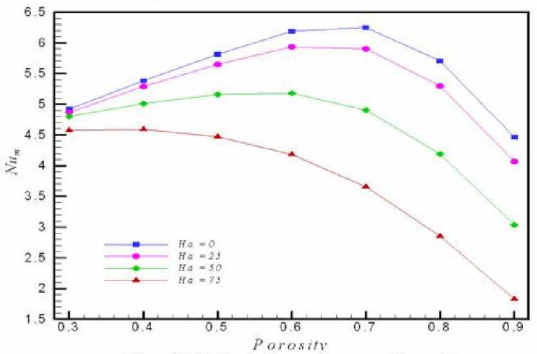

Fig. (17) Variation of mean Nusselt number with porosity at Da=1.E-3

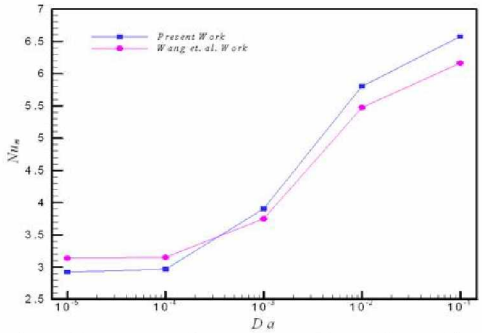

Fig. (18) Comparison of mean Nusselt number with Darcy number at Ha=0 & ε=0.9 with Wang et. al. work